1. Experimental Setting

Setting as shown in Figure S1: Commercial 400 mesh TEM copper grid deposited with a thin film of silicon monoxide (10nm-30nm) on one side was used. A single-crystal copper plate in {111} orientation with one side polished to mean surface roughness Ra < 3 nm was used as a laser energy absorber. The copper grid was attached to the copper plate with the silicon monoxide facing to the polished copper surface. A piece of steel and a neodymium magnet sandwiched the copper grid and copper substrate. The magnetic force was designed to make sure a firm attachment between the silicon monoxide thin film and polished copper surface. There was a circular opening on the steel so could laser can directly irradiate through the silicon monoxide thin film and its energy was absorbed by the copper substrate. The diameter of the circular opening was 2.5 mm. The opening area was designed to be significantly smaller than the square shape laser energy input (9.0 mm by 9.0 mm) so that heat transfer condition on the copper grid can be thought as identical. Both the steel and neodymium magnet were entirely wrapped by acrylic tape in order to prevent side-reactions between them and the solution.

Laser: Q-switched Nd:YAG laser (wavelength 1064nm, pulse duration 5 ns, randomly polarized) was used as the laser source. The laser beam passed through an engineered diffuser and a plano-convex lens. At the location where laser met the copper plate, the laser beam was in a 9.0 mm by 9.0 mm square shape. Commercial engineered diffuser was used in order to even the laser energy throughout the beam cross-section (top-hat shape). The energies of the laser pulse were measured by a laser power meter. The laser pulse energies mentioned in this report are all full beam energies (9.0 mm by 9.0 mm in size). For example, the areal energy density of the 220 mJ laser pulse is 0.22 J/ 0.81 cm^2 or 0.27 J/cm^2. The laser was warmed up sufficiently to make sure the stability of the energy output: the random variation of energy output from laser was less than 1% of the energies used in this study. During multiple pulses experiment, the laser repetition rate was 5 Hz.

Selection of the laser pulse width. Crystal nucleation takes place within a time window from nanoseconds to seconds. [1] For iron oxide nanoparticle, molecular dynamics simulations showed the nucleation process lasted for tens of nanoseconds. [2] Thus, a laser with pulse width of 5 ns was used in this study. It was long enough to initiate the nucleation process but short enough to prevent it from triggering the aging process. As shown in Figure S3, the effective laser heating duration in this work was about 8 ns. The relatively fast cooling was attributed to the usage of copper plate with a good thermal conductivity.

Selection of the laser wavelength. Direct laser heating of nuclei such as Fe_2O_3 would accelerate the order development process during nucleation. In order to prevent the acceleration and reveal details during the order development, it was designed to limit the laser-iron oxide interaction. The bandgap of Fe_2O_3 is 2.1 eV. Thus a wavelength of 1064 nm (corresponding to 1.2 eV) was chosen. Specifically, the absorption coefficient of iron oxide (hematite) is about $3\times10^2 cm^{-1}$ @ 1064nm.[3] In comparison, the absorption coefficient of copper at 1064 nm wavelength is $8\times10^5 cm^{-1}$@ 1064nm. Therefore, laser wavelength of 1064 nm was chosen. It was believed the laser energy was absorbed by the copper while the absorption by iron oxide was negligible.

Absorption of 1064 nm laser light by water. Distilled water absorbs 1064nm laser light. The refractive indices of distilled water for 1064 nm wavelength is 1.2×10^{-6}.[4] Accordingly, the optical penetration depth is $l_\alpha = \alpha^{-1} = \frac{\lambda}{4\pi k} = 7\ cm$, where α is absorption coefficient, λ is the wavelength and k is the refractive indices. In order to minimize the water absorption, we set the distance between the liquid surface and the copper substrate to be 0.4 cm. Namely, laser travelled about 1/18 of its penetration depth in water and then was absorbed by the copper substrate. Therefore we believe the laser energy was mainly absorbed by the copper substrate, instead of water.

Chemicals: 2.48 mM Iron (III) nitrate nonahydrate was dissolved in 50 mL deionized water and nitric acid was added to the solution till the pH reaches 0.8. The pH value was measured by a Hanna pHep 5 pH meter with an accuracy of ± 0.05. The pH value was designed to be as low as 0.8 so that no spontaneous precipitation took place after 7 minutes. The copper grid and copper substrate setting was put inside the Iron (III) solution and irradiated by certain number of laser pulses. The duration of copper grid inside Iron (III) solution for all samples was 7 minutes. It was designed so that time is a constant for all different conditions. After 7 minutes, the copper grid and copper plate assembly was removed from the Iron (III) solution and immediately rinsed by acetone for 2 minutes. This step was designed to rinse off the water as well as the unreacted Iron (III) ions from the copper grid. After the rinse, the copper grid was detached from the copper plate and dried in air. Then it was investigated by a Titan 80 300 kV transmission electron microscope (TEM).

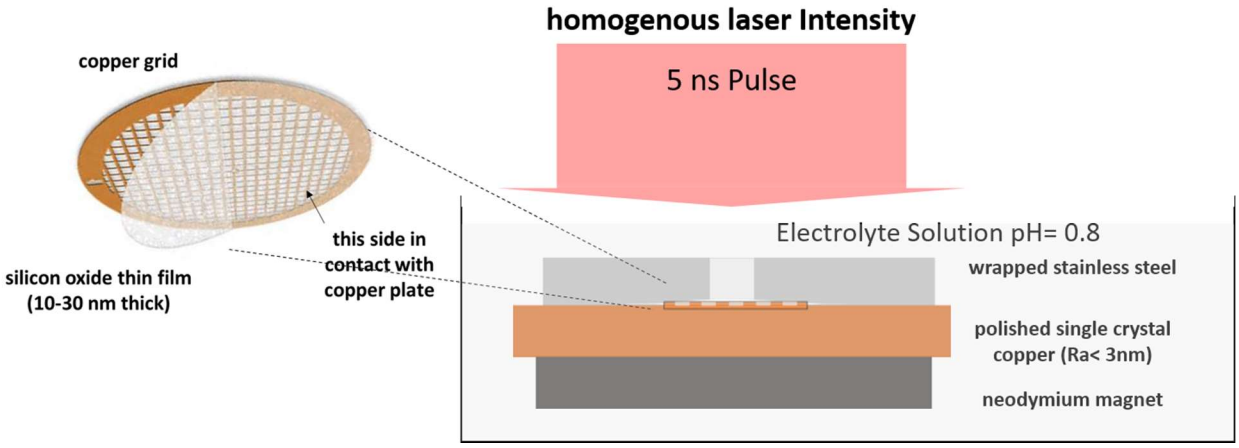

Figure S1. Schematic illustration of the experimental setup.

2. Instability/transformation of the amorphous particle under TEM electron beam irradiation

Instability/transformation of the amorphous particle under TEM electron beam irradiation is demonstrated in Figure S2 A-E. Figure S2A shows the initial amorphous structure by a single pulse laser irradiation at 150 mJ and rinsed dry. After 1 minute of exposure of the amorphous phase under e-beam, the extrusion at the top of particle and a black dot indicated by the blue arrow disappeared, as shown in Figure S2B. In addition, the boundary of the particle became less clear. After 2 minutes, as shown in Figure S2C, the boundary of amorphous particle became harder to recognize. On the other side, new dots appeared within the amorphous particle. The high resolution TEM image of Figure S2D showed a newly formed dot with an average lattice spacing of 0.208 nm, which matched the spacing of (202) planes of hematite. It implied that the electron beam induced the deposition of crystalline hematite with the amorphous particle as a material source. After 5 minutes, the transformation was complete as shown in Figure S5E. The amorphous particle shown in Figure S2A disappeared entirely. Instead, 10 new hematite nanocrystals were produced at the same location. During the whole transformation, a black dot pointed by the red arrows did not disappear, whereas the dots pointed by the blue arrows vanished at the beginning. It suggested the denser configurations represented by the dots were not the same and some were more stable than the others. Although the details (e.g. bonding) of the amorphous particle were difficult to study due to its instability, the re-deposition of hematite within TEM vacuum column indicated that the amorphous particle composed of disordered iron (oxy)hydroxide polymers.

The transformation process of the amorphous particle under electron beam irradiation shares some similarities with that of amorphous particle under multiple pulses laser irradiation as shown in Figure 3. In both situations, external energies were provided which lead to the transformation processes of the amorphous particles. During the processes, the volume of the amorphous phase changed and new crystalline structures formed. The transformation processes in both situations suggest the instability of amorphous particle under external energy input.

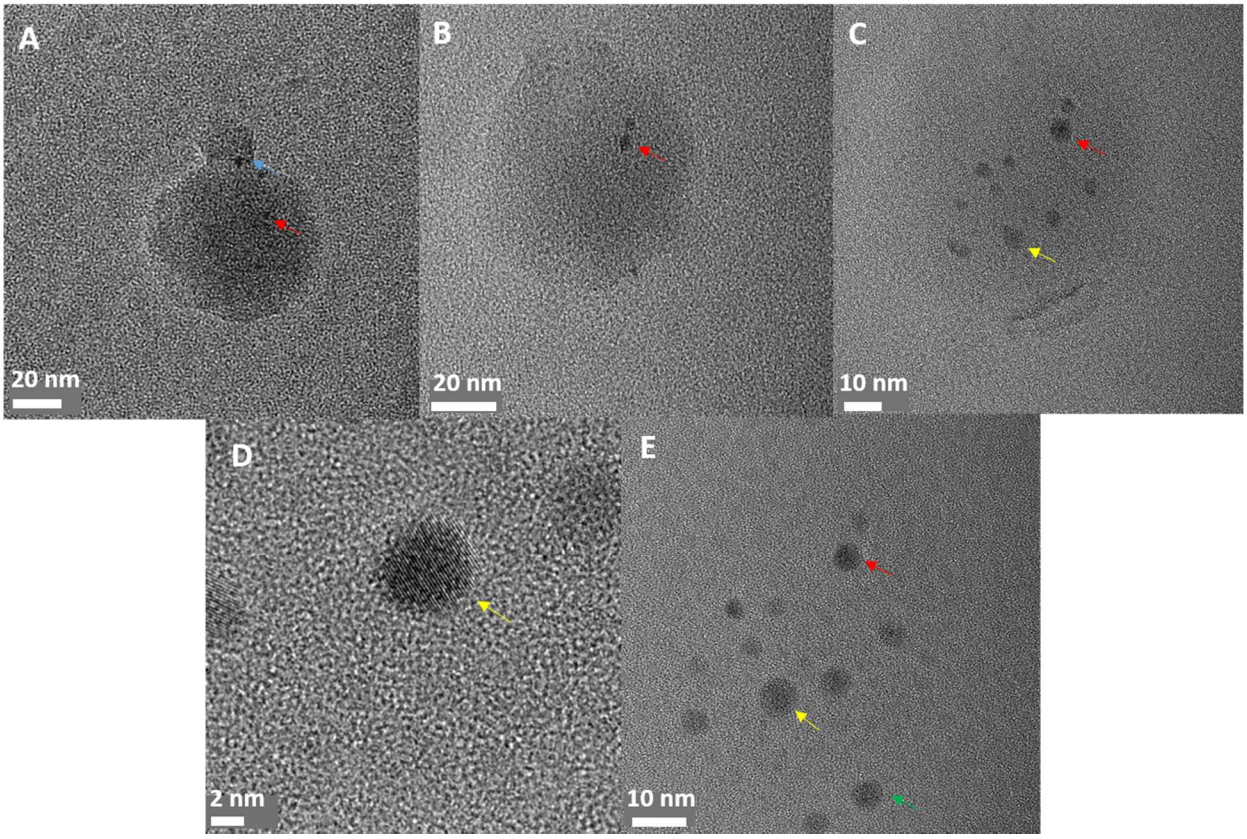

Figure S2. The effect of electron beam irradiation during TEM imaging: A. the original sample rinsed and dried, B. after 1 minute, C. after 2 minutes, D. high resolution TEM image of C, and E. after 5 minutes electron beam exposure.

3. Estimation of the size of critical nucleus of hematite

The solution contained 2.48 mM Iron (III) nitrate nonahydrate and the pH value was 0.8. The temperature was 298K. At this condition, the solubility of Iron(III) was estimated to be 0.8 mM. [5] The average atomic volume for hematite is $5.7\times10^{-29}m^3$. [6] The free-energy gain per unit volume on formation of the hematite nucleus g_v can be described as: [7]

$$g_v = \left[k_B T ln\left(\frac{C}{C_s}\right)\right]/V_m \quad (1)$$

where k_B is the Boltzmann constant, T is the temperature, C is the solute concentration, C_s is the solubility and V_m is the atomic volume. In this work, the free-energy gain per unit volume on formation of the hematite nucleus g_v was estimated to be $8.3\times10^7 J/m^3$.

According to the classical nucleation theory, nuclei that are bigger than the critical size grow spontaneously while smaller ones dissolve. The critical radius r^* can be described as:

$$r^* = \frac{2\gamma}{g_v} \quad (2)$$

where γ is the surface energy. The surface energy of hematite is 0.75 Jm^{-2}. [8] Thus the critical radius was estimated to be 18 nm, or the critical size was 36 nm.

4. Discussion of the laser effect

Photochemical process. For a purely photochemical process, the temperature of system remains unchanged under laser irradiation. Laser induced photochemical process is typically based upon electronically excited molecules and photofragments of them.[9] In this work, the laser wavelength was 1064 nm (1.2 eV). The solution with 2.48 mM Iron (III) nitrate nonahydrate at 0.8 pH value was colorless and transparent to visible light (400nm-700nm). Also, the bandgap of hematite is 2.1 eV which significantly larger than the laser photon energy.

In addition, we have conducted control experiment of passing laser light through the same solution without irradiating onto the copper grid and copper substrate assembly. The laser pulse energy was 220 mJ. Repetition rate was 5 Hz. And total irradiation time was 7 minutes. No crystal can be found. Therefore, we believe the laser induced photochemical process can be ignored.

The nonphotochemical laser induced nucleation (NPLIN) process. Nucleation of urea took place when the supersaturated solution was exposed to pulses of laser light. The term NPLIN was introduced to describe the phenomenon. [10] It was found the formed crystallite were aligned with the direction of the electric field of linearly polarized light. The mechanism were explained based on optical Kerr effect. However, a recent work demonstrated that urea crystal are not aligned with the direction of the electric field due to NPLIN. [11] In the NPLIN studies, laser light was circularly or linearly polarized and multiple pulses were used to initiate the nucleation process.

In this work the laser light was randomly polarized and one nanoseconds pulse was sufficient to initiate the nucleation process. Moreover, control experiment was conducted. Laser light passed through the same solution without irradiating onto the copper grid and copper substrate assembly. The laser pulse energy was 220 mJ. Repetition rate was 5Hz. And total irradiation time was 7 minutes. No crystal can be found. We therefore believe the NPLIN process can be ignored.

Laser shock wave induced crystallization. High intensity focused laser pulses created compression waves within liquid or onto the wall of a container. Crystals were formed as a result of shock waves. [12] To initiate laser shock wave induced crystallization, laser power intensity in the scale of 1×10^{12} W/cm^{-2} was used. A study showed the temperature inside a laser induced bubble reached a value that was significantly higher than 2000 K. [13]

In this work, laser power intensity less than 5×10^{7}W/cm^2 was used (lower than those in NPLIN, i.e. 2×10^{8}W/cm^2 [11]) The peak temperature of the copper surface during laser irradiation was estimated to be 389 K. We therefore believe the laser shock wave induced crystallization mechanism can be ignored.

Thermal process. The laser energy was absorbed by the copper grid and copper plate assembly**.** According to the calculation, the temperature of the surface of the copper rose more than 50 K due to the laser irradiation. Previous studies on laser induced formation of metal oxides in solution suggested the phase transformation was due to thermal effects. Evidences included: 1) the size of metal oxide deposition was larger than the laser beam.[14] 2) Laser irradiating to the back of an opaque substrate caused deposition on the front side of the substrate. [15]

In this work, the ferric nitrate solution was colorless at the pH value of 0.8. This suggested that the hydrolysis of Iron (III) did not occur and the iron cations existed as hexcoorditated aquo complexes. However, heating of the solution to more than 50 Celsius can facilitate the hydrolysis process for Fe (III). [16] This is because the entropy increases as a result of hydrolysis of trivalent metal elements. The forced hydrolysis of acidic Fe(III) solution leads to the precipitation of hematite. [17]

Thus we believe the formation of iron oxide was due to the laser induced thermal effect.

5. Estimation of the peak temperature and heating duration by laser irradiation

During the experiment, laser light passed through a transparent liquid and heated up the surface of a thick single crystal copper substrate. Considering the energy flux into the liquid medium was at the scale of 10 W/cm^2 [9]while the energy flux by laser irradiation was at the scale of 1×10^7 W/cm^2, we ignored the energy loss to liquid medium in the calculation. Engineered diffuser was used to even the laser energy throughout the beam cross-section (top-hat shape). The temperature rise was analytical solved based on a model for pulsed laser uniform irradiation onto semi-infinite substrate with finite absorption[9]:

$$\Delta T(0,t) = \frac{I_a}{\kappa}\{\frac{l_T}{\sqrt{\pi}} - \frac{1}{\alpha}[1 - exp\left(\frac{\alpha l_T}{2}\right)^2 erfc(\frac{\alpha l_T}{2})]\} \quad (3)$$

Note when z>10, as in the case of the experiments reported here (z=58) , erfc (z)→0. The temperature rise can be simplified as:

$$\Delta T(0,t) = \frac{I_a}{\kappa}(\frac{l_T}{\sqrt{\pi}} - \frac{1}{\alpha}) \quad (4)$$

$$l_T = 2(Dt)^{\frac{1}{2}}$$

where ΔT is the temperature rise, t is the time, I_a is the absorbed laser light intensity(in this case, $I_a = \frac{x(1-R)}{0.81cm^2 \cdot 5\times10^{-9}s}$, where x is the laser energy input and R is the reflectivity), κ is the thermal conductivity, D is the thermal diffusivity and α is the optical absorption coefficient.

The specific data for laser heating (1064nm wavelength) of copper plate are used according to the reference[9]

Property	Value
R	0.92
κ	4.0 W/cmK
α	7.7×10^5cm^{-1}
D	1.14 cm^2/s
t	5×10^{-9}s

The background temperature was 298K. The laser pulse energies mentioned in this report are all full beam energies (9.0 mm by 9.0 mm in size). Thus the peak temperatures $\Delta T(0,5ns)$on the surface of copper substrate by different energy inputs were:

Laser Energy Input (mJ)	Surface Temperature (K)
220	389
190	376
160	364
150	360
120	347

The Boltzmann thermal energy was defined as R×T (R is the ideal gas constant and T is the temperature) and the energies due to different laser energy inputs are:

Laser Energy Input (mJ)	T (K)	Thermal Energy RT (kJ/mol)
220	389	3.2
190	376	3.1
160	364	3.0
150	360	3.0
120	347	2.9

The peak temperature rise due to 220 mJ laser heating was calculated to be 389 K which was sufficient to meet the temperature condition required for hematite crystallization (>90°C).[18]

It was found hematite crystals with average size of 49 nm were synthesized in ferric chloride solution at the temperature of 393 K by microwave heating[19]. The finding is comparable with the estimation that hematite crystals with average size of 51 nm formed at the temperature of 389 K by 220 mJ laser heating. We believe the calculation of temperature rise shown here provides a reasonable estimation about the actual temperature in the experiments.

The cooling process after the laser pulse can be described by[9]:

$$\Delta T(z,t) = \frac{2I_a D^{1/2}}{\kappa}\left[t^{\frac{1}{2}} ierfc\left(\frac{z}{2(Dt)^{\frac{1}{2}}}\right) - (t-\tau_l)^{\frac{1}{2}} ierfc\left(\frac{z}{2D^{\frac{1}{2}}(t-\tau_l)^{\frac{1}{2}}}\right)\right] \quad (5)$$

Note that $ierfc(z=0) = 1/\sqrt{\pi}$.

$$\Delta T(0,t) = \frac{2I_a D^{1/2}}{\kappa\sqrt{\pi}}\left[t^{\frac{1}{2}} - (t-\tau_l)^{\frac{1}{2}}\right] \quad (6)$$

where ΔT is the temperature rise, t is the time, z is the distance from the surface, I_a is the absorbed laser light intensity, κ is the thermal conductivity, D is the thermal diffusivity and τ_l is the time duration of laser pulse.

At the copper surface z=0, with 5 ns laser pulse duration and at 220 mJ laser pulse energy, the result of the temperature change is:

Time (ns)	Temperature (K)
6	358
7	349
8	343
15	327
30	318
2×10^8	298

According to the calculation, at the 8th ns, the temperature rise (ΔT= 45 K) was less than the half of that immediately after the laser pulse (ΔT= 91 K), which was also less than the maximum temperature rise due to 150 mJ laser pulse irradiation(ΔT= 62 K). We assign 8 ns as the laser heating duration.

By a 220 mJ laser pulse irradiation, the estimated temperature of the copper top surface as a function of time (t) is shown in Figure S3.

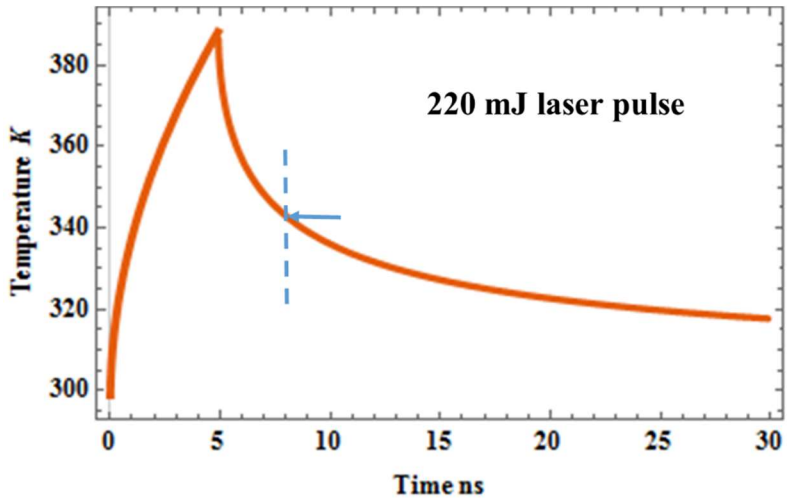

Figure S3. Estimated temperature of the copper top surface as a function of t, when the laser energy is 220 mJ.

Negligible heat accumulation effect during multiple pulse experiment.

According to the calculation, at the 0.2^{th} s, namely the moment when the next pulse arrives in multiple pulse experiment, the temperature change was estimated to be $< 10^{-5}$ K. The small change was believed to attribute to the low pulse frequency of 5 Hz and the usage of copper plate with good thermal conductivity. Therefore, heat accumulation effect during multiple pulse irradiation is negligible.

ESI References:

[1] G. C. Sosso, J. Chen, S. J. Cox, M. Fitzner, P. Pedevilla, A. Zen, A. Michaelides, *Chem. Rev.* **2016**, *116*, 7078–7116.

[2] H. Zhang, G. A. Waychunas, J. F. Banfield, *J. Phys. Chem. B* **2015**, *119*, 10630–42.

[3] I. Balberg, H. L. Pinch, *J. Magn. Magn. Mater.* **1978**, *7*, 12–15.

[4] L. Kou, D. Labrie, P. Chylek, *Appl. Opt.* **1993**, *32*, 3531.

[5] J.-H. Jang, B. A. Dempsey, W. D. Burgos, *Environ. Sci. Technol.* **2007**, *41*, 7303–7308.

[6] R. M. Cornell, U. Schwertmann, *The Iron Oxides: Structure, Properties, Reactions, Occurrences and Uses*, John Wiley & Sons, **2006**.

[7] J. Baumgartner, A. Dey, P. H. H. Bomans, C. Le Coadou, P. Fratzl, N. a J. M. Sommerdijk, D. Faivre, *Nat. Mater.* **2013**, *12*, 310–4.

[8] A. Navrotsky, *ChemPhysChem* **2011**, *12*, 2207–2215.

[9] D. Bauerle, *Laser Processing and Chemistry*, Springer-Verlag Berlin Heidelberg, **2011**.

[10] B. A. Garetz, J. E. Aber, N. L. Goddard, R. G. Young, A. S. Myerson, *Phys. Rev. Lett.* **1996**, *77*, 3475–3476.

[11] Y. Liu, M. R. Ward, A. J. Alexander, *Phys. Chem. Chem. Phys.* **2017**, *19*, 3464–3467.

[12] N. Mirsaleh-Kohan, A. Fischer, B. Graves, M. Bolorizadeh, D. Kondepudi, R. N. Compton, *Cryst. Growth Des.* **2017**, *17*, 576–581.

[13] I. Akhatov, O. Lindau, A. Topolnikov, R. Mettin, N. Vakhitova, W. Lauterborn, *Phys. Fluids* **2001**, *13*, 2805–2819.

[14] Z. Liu, C. Richard Liu, *J. Micro Nano-Manufacturing* **2014**, *2*, 011007.

[15] J. Bin In, H.-J. Kwon, D. Lee, S. H. Ko, C. P. Grigoropoulos, *Small* **2014**, *10*, 741–9.

[16] J.-P. Jolivet, M. Henry, J. Livage, *Metal Oxide Chemistry and Synthesis: From Solution to Solid State*, Wiley, **2000**.

[17] U. Schwertmann, R. M. Cornell, *Iron Oxides in the Laboratory: Preparation and Characterization*, VCH, **1991**.

[18] J.-P. Jolivet, C. Chanéac, E. Tronc, *Chem. Commun.* **2004**, *0*, 477–483.

[19] H. Katsuki, S. Komarneni, *J. Am. Ceram. Soc.* **2004**, *84*, 2313–2317.